Journal of Solid State Chemistry 226 (2015) 243–249

Contents lists available at ScienceDirect

Journal of Solid State Chemistry

journal homepage: www.elsevier.com/locate/jssc

Synthesis and photoluminescence properties of Dy^{3+} doped white light emitting $CdTa_2O_6$ phosphors

Mustafa İlhan [a,*], Mete Kaan Ekmekçi [b]

[a] Department of Metallurgical and Materials Engineering, Marmara University, Göztepe Kampüsü, Kadıköy, 34722 İstanbul, Turkey
[b] Department of Chemistry, Marmara University, Göztepe Kampüsü, Kadıköy, 34722 İstanbul, Turkey

ARTICLE INFO

Article history:
Received 17 October 2014
Received in revised form
24 February 2015
Accepted 25 February 2015
Available online 13 March 2015

Keywords:
$CdTa_2O_6$
XRD–SEM
Dy^{3+}
Photoluminescence
W-LEDs

ABSTRACT

The undoped and $CdTa_2O_6$:Dy^{3+} ($0.2 \le x \le 2.0$ mol%) phosphors were synthesized at 1100 °C for 12 h by the conventional solid state reaction method. The synthesized $CdTa_2O_6$:Dy^{3+} phosphors were characterized by X-ray diffraction (XRD), Scanning electron microscopy (SEM), Energy dispersive spectroscopy (EDS) and Photoluminescence (PL) analyses. The PL spectra showed the presence of excitation peaks between 310 and 440 nm due to the 4*f*–4*f* transitions of Dy^{3+}. The emission of Dy^{3+} ions at 353.0 nm excitation was observed at 487.1 nm (blue) and 577.8 nm (yellow) due to the $^4F_{9/2} \rightarrow {}^6H_{15/2}$ transitions and $^4F_{9/2} \rightarrow {}^6H_{13/2}$ transitions, respectively. The PL analysis results also showed that the emissions increase with the increasing Dy^{3+} ion content. The emissions increased with the doping concentration of up to 1 mol%, and above this level decreased due to concentration quenching effect. The CIE chromaticity color coordinates (*x*,*y*) of the $CdTa_2O_6$:Dy^{3+} phosphors were found to be in the white light region of the chromaticity diagram.

© 2015 Elsevier Inc. All rights reserved.

1. Introduction

Rare earth (RE^{3+}) doped materials have wide range of applications in the field of solid state lighting, display, and laser technologies. The phosphor material should have good absorption and emission properties, good thermal and chemical stability, minimal thermal quenching and high quantum yield. This material should also be preferably inexpensive and easy to fabricate [1–4]. Trivalent RE^{3+} ions having 4*f*–4*f* inner-shell transitions possess specific advantage features such as high luminescence yield, narrow emission line, and long decay time constant. Moreover, in recent years, white light emitting diodes (W-LEDs) have been targeted as next generation solid state lighting sources due to the advantages of long lifetime, energy saving, high efficiency, reliability and environmentally friendly properties [5–7]. Currently, trivalent dysprosium ion (Dy^{3+}) doped phosphors are of great interest because of white light emission characteristic. Usually, Dy^{3+} ions have two dominant emission bands: one is in blue region (470–500 nm) due to $^4F_{9/2} \rightarrow {}^6H_{15/2}$ transition and the other is in yellow region (570–600 nm) corresponding to the $^4F_{9/2} \rightarrow {}^6H_{13/2}$ transition [8–10].

Cadmium contained quantum dots (QDs) have attracted enormous interests in the last decade as a novel class of material due to their special properties and a wide area of potential applications such as biomedical screening, light-emitting diodes (LEDs), solar cells, optics, and biosensors [11–15]. On the other hand, the inherent toxicity of cadmium limits their applications especially in the biomedical and industrial areas. For example, the cytotoxicity and genotoxicity of QDs with a Cadmium selenide/Zinc sulfide (CdSe/ZnS) core/shell for applications in cancer therapy has been discussed recently [16]. However, cadmium based phosphors have been put into use recently since they provide high levels of brightness. This leads to reduction in the need for high levels of X-ray doses. Accordingly, the risk of health problems can be minimised [11,17].

Cadmium tantalates were investigated due to photocatalytic [18] and neutron absorption properties [19] of $Cd_2Ta_2O_7$ compound. However, there has been no work found reported about $CdTa_2O_6$ in the literature. On the other hand, $CdNb_2O_6$ was studied recently because of its ion irradiation [20], ferroelectric [21] and luminescence properties [22,23]. In this context, ternary oxides of general formula AB_2O_6 ($A = M^{2+}$, B = Nb, Ta), crystallizing in the columbite or tri-rutile structure, have attracted great attention because of their microwave dielectric properties [24,25]. In the AB_2O_6 columbite structure, the *A* and *B* cations are at the center of octahedra surrounded by six oxygen atoms. The AO_6 and BO_6 octahedra form independent zig-zag chains by sharing edges, and the chains are connected by sharing corners in the order AO_6 chain-BO_6 chain-BO_6 chain. In the fully ordered state, this forms repeating *ABBABB* octahedral layers, with an orthorhombic structure with space group *Pbcn*, first solved by Sturdivant. The unit

* Corresponding author. Tel.: +90 216 348 02 92 609; fax: +90 216 345 01 26.
E-mail address: mustafa.ilhan@marmara.edu.tr (M. İlhan).

http://dx.doi.org/10.1016/j.jssc.2015.02.023
0022-4596/© 2015 Elsevier Inc. All rights reserved.

cell is orthorhombic and space group no. 60 (either *Pbcn* or *Pcan*) for the columbite niobates or tantalates [26,27].

There are several routes to synthesise the tantalates, such as conventional solid state reaction [28,29] hydrothermal synthesis [30–32], pulsed laser deposition [33], molten salt method [34], polymeric precursor method [35], ceramic flux [36,37], precipitation [38] traditional glass fusion casting method [39], and mechanochemical synthesis [40,41].

The synthesis and photoluminescence properties of Dy^{3+} doped $CdTa_2O_6$ ceramics phosphors were investigated. Detailed microstructural characterization and photoluminescence properties of the samples were performed using the XRD, SEM, EDS and fluorometric analyses.

2. Materials and methods

Pure and $CdTa_2O_6$:xDy^{3+} ($0.2 \le x \le 2.0$ mol%) materials were synthesized by a solid state reaction method. $Cd(NO_3)_2 \cdot 4H_2O$ with purity of 99% (Sigma-Aldrich) and Ta_2O_5 with purity of 99.9% (Alfa Aesar) powders were used as starting materials. Dy_2O_3 with purity of 99.9% (Alfa Aesar) was used as a dopant. $Cd(NO_3)_2 \cdot 4H_2O$ and Ta_2O_5 powder mixtures were prepared according to $CdTa_2O_6$ stoichiometry. This powder mixture was doped with Dy_2O_3. The doped powder mixtures were homogenized in agate mortar. Then these powders were sintered at 1100 °C for 12 h under air atmosphere in an electric furnace.

The phase compositions and crystallography parameters in sintered samples were determined by X-ray diffractometer (XRD, Rigaku Corp., D-MAX 2200) using Cu*K*α radiation at a scan rate of 2°/min between 20 and 65° and Ni filter. The morphology and elemental composition of the sintered powders were investigated by Scanning electron microscopy (SEM, JEOL Ltd., JSM-5910LV) equipped with Energy dispersive spectroscopy (EDS, OXFORD Industries INCAx-Sight 7274; 133-eV resolution 5.9 keV) after Au/Pd (gold/palladium) coating. Photoluminescence (PL) measurements, excitation and emission spectra were recorded by using a Scinco floromaster-FS/2 model fluorometer with a Xe-arc lamp (150 W) as excitation source. Ultraviolet irradiation was studied by using an UV lamp (CAMAG) of 254.0 nm and 365.0 nm excitation wavelenghts. All of the photoluminescence measurements were performed at room temperature.

3. Results and discussion

3.1. X-ray diffraction and SEM–EDS analyses

Fig. 1 shows the XRD patterns of pure and doped powders. XRD pattern of $CdTa_2O_6$ samples sintered at 1100 °C for 12 h included a $CdTa_2O_6$ single phase (JCPDS card no. 39-1431) which was obtained up to 1.0 mol% Dy^{3+}. However, minor differences were observed in the relative intensity of characteristic diffraction peaks at the Dy^{3+} concentrations above 1.0 mol%. It was found that $Cd_2Ta_2O_7$ (JCPDS card no. 34-0405) and Ta,O (hexagonal δ-Ta_2O_5) (JCPDS card no. 19-1299) [42] phases were formed at 1.5 and 2 mol% doping concentrations of Dy^{3+}, respectively. XRD analysis indicated that $CdTa_2O_6$ samples crystallized in orthorhombic symmetry with space group *Pbcn*(60) having the columbite type structure. It was reported by Santos et al.[27] that, $CdTa_2O_6$ columbite structure has cell parameters of $a=14.785$ Å, $b=5.851$ Å, $c=5.146$ Å, and $V=445.2$ Å^3. $CdTa_2O_6$ structure could be illustrated as shown in Fig. 2. Refined and calculated cell parameters of all doped powders were presented in Table 1. In the columbite structure, based on the effective ionic radius of cations with coordination numbers (C.N.), it was assumed that, Dy^{3+} ions ($r=0.912$ Å, for C.N. 6) may replace Cd^{2+} ions ($r=0.95$ Å, for C.N. 6). It is obvious that Dy^{3+} ions will not be able to replace Ta^{5+} ions

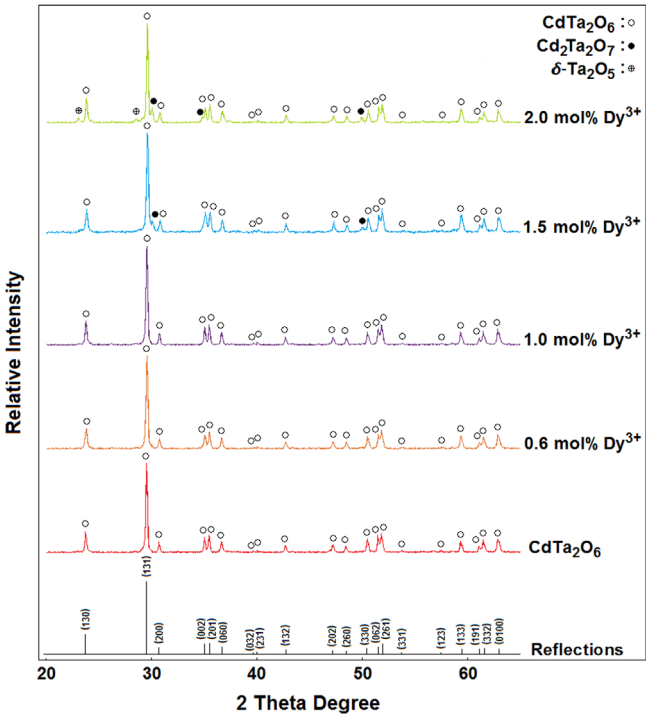

Fig. 1. X-ray diffraction patterns of pure $CdTa_2O_6$ and doped with Dy^{3+} concentrations of 0.6, 1.0, 1.5 and 2.0 mol%.

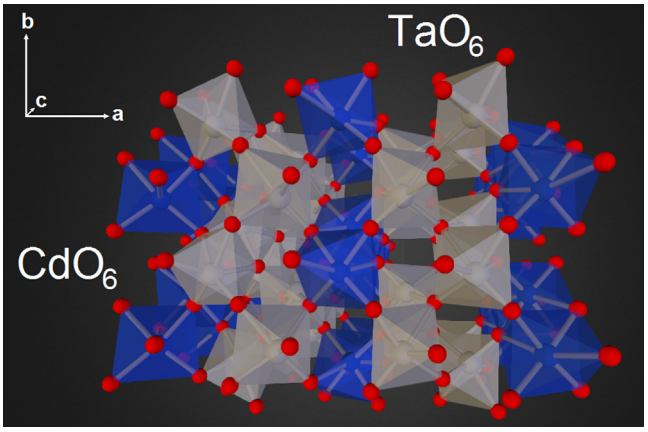

Fig. 2. Schematic illustration of the crystal structure of $CdTa_2O_6$.

($r=0.64$ Å, for C.N. 6). XRD lattice parameters exhibited decreases up to 2.0 mol% doping concentration. It was observed that shrinkage of the lattice occurred due to Dy^{3+} ions entries in the lattice up to 2 mol % where Dy^{3+} ions were successfully located in the $CdTa_2O_6$ lattice. Trivalent dysprosium ions could be located in the Cd^{2+} sites of lattice due to size effect ($r_{cation}/r_{anion} \approx 0.65$, the C.N. of Dy^{3+} is 6) and attractive ionic forces between anions and cations where the lattice structure was shrinking up to 2 mol% Dy^{3+} doping concentration.

SEM and EDS investigations were also in agreement with the XRD results. Fig. 3(a–d) shows the SEM micrographs of pure and 0.6, 1.0 and 2.0 mol% Dy^{3+} doped samples. SEM analysis revealed that the grain size of $CdTa_2O_6$ decreased slightly for doped samples with the increasing concentrations of Dy^{3+} ions up to 2 mol%. The structures of Dy^{3+} doped $CdTa_2O_6$ powders exhibited oval like shapes and grain sizes varied between 0.3 and 2.0 μm. SEM and EDS analyses also revealed differences in the elemental compositions between $CdTa_2O_6$, $Cd_2Ta_2O_7$ and δ-Ta_2O_5 grains. EDS analyses was performed at 10 kV of SEM acceleration voltage in order to detect the smaller grains present at surface. A SEM micrograph

and EDS spectrums of 2.0 mol% Dy^{3+} doped sample were given in Fig. 4(a–d). In EDS analyses, atomic ratio of Ta/Cd was found to be about 2:1 for $CdTa_2O_6$ large grains (point 1 in Fig. 4b). As it can be seen from the (point 2 in Fig. 4c), Ta/Cd ratio decreased for small grains of $Cd_2Ta_2O_7$ that formed mostly between $CdTa_2O_6$ grains. The δ-Ta_2O_5 phase was also detected on the $CdTa_2O_6$ grains depending on the increase of Ta/Cd ratio (point 3 in Fig. 4d).

From the XRD and SEM–EDS results, it can be claimed that, some Dy^{3+} ions in the columbite structure may replace Cd^{2+} cations leading to the formation of $Cd_2Ta_2O_7$. Furthermore, some of the Ta^{5+} cation sites in $CdTa_2O_6$ structure may also be distorted at 2 mol% doping concentration due to the presence of hexagonal δ-Ta_2O_5 phase. Although the incorporation of Dy^{3+} ions did not cause the change in the single phase structure of $CdTa_2O_6$ up to 1.0 mol% concentration, the incorporation of Dy^{3+} ions will affect the charge compensation in the structure. Therefore, a changing charge balance in the lattice could be based on mostly the loss of Cd^{2+} cations and small amount of Ta^{5+} cations.

Table 1
Crystallography and lattice parameters.

Crystallography and refinement data				
	Formula	$CdTa_2O_6$		
	Crystal system	Orthorhombic		
	Space group	*Pbcn*(*60*)		
	a (Å)	14.785	[27]	
	b (Å)	5.851	[27]	
	c (Å)	5.146	[27]	
	V (Å^3)	445.2	[27]	
	Z	4	[27]	
	2θ range (deg)	20–65		
	Step (deg/min)	2		
	Program	MDI Jade 6.5		
Dy^{3+} concentration	Cell data			
	a (Å)	*b* (Å)	*c* (Å)	*V* (Å^3)
0.2	14.6541 (5)	5.8123 (4)	5.1245 (3)	436.47
0.6	14.6387 (7)	5.8056 (4)	5.1164 (4)	434.82
1.0	14.6213 (7)	5.7962 (5)	5.1007 (6)	432.61
1.5	14.6123 (5)	5.7903 (7)	5.0178 (3)	424.55
2.0	14.6121 (6)	5.7821 (6)	4.9929 (7)	421.84

3.2. *Photoluminescence analyses of pure $CdTa_2O_6$ and Dy^{3+} doped $CdTa_2O_6$ phosphors*

Fig. 5 shows the excitation and emission spectra of pure $CdTa_2O_6$ at 224.6 nm and 388.9 nm wavelength, respectively. The excitation spectrum has been attributed to the O^{2-}–RE^{3+} charge transfer band (CTB) which is caused by the electron transfer from filled 2*p* orbital of O^{2-} ions to vacant 4*f* orbital of RE^{3+} ions. Emission of $CdTa_2O_6$ also showed a broad and strong peak at 388.9 nm. In the columbite structure, edge-shared TaO_6 groups are the efficient luminescent centers for the host emission which attributed to self-trapped exciton recombination [43]. On the other hand, $CdTa_2O_6$ may also act as antennas for RE^{3+} ions because of strong charge transfer absorptions of tantalates [28].

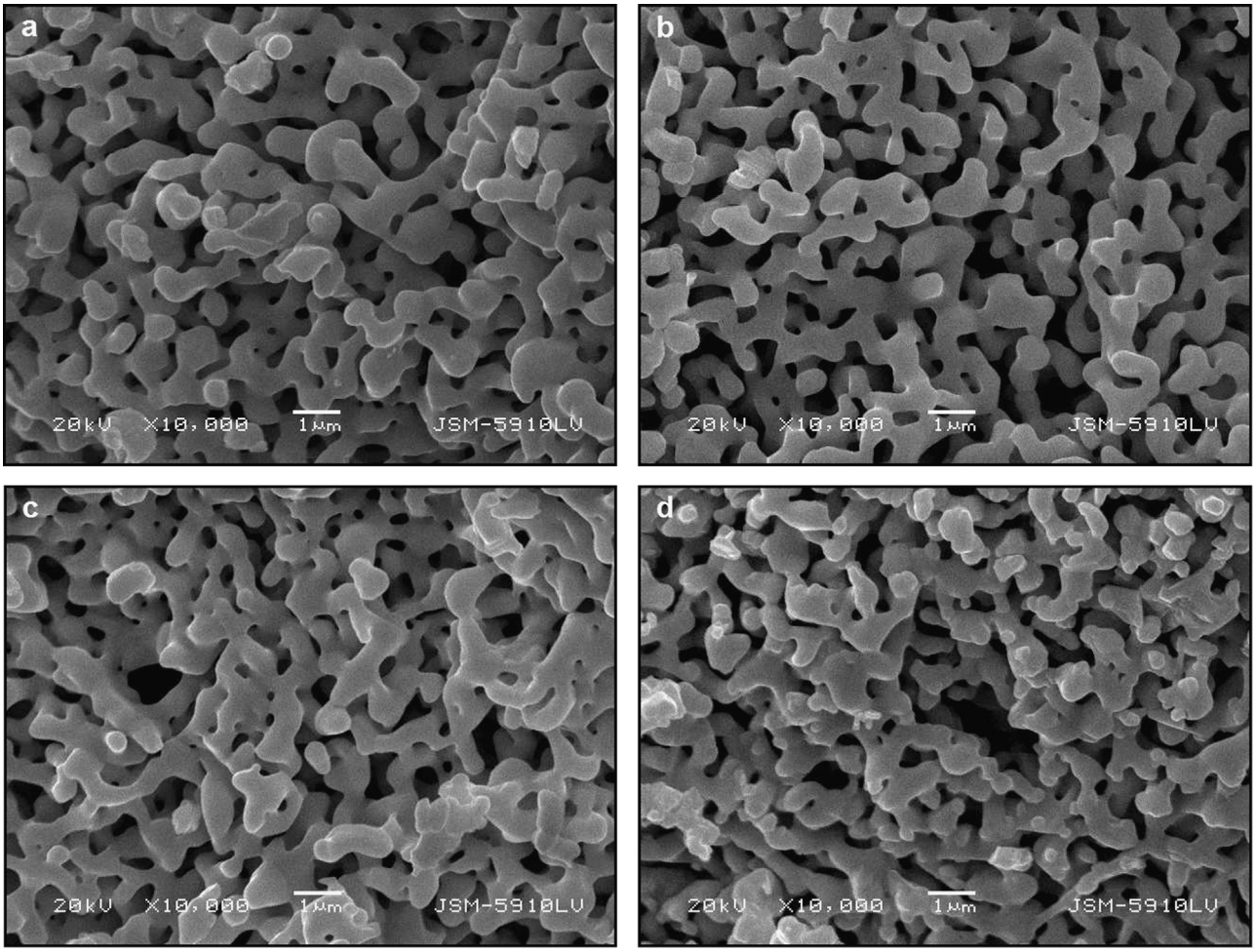

Fig. 3. SEM micrographs at × 10 000 magnification of (a) pure $CdTa_2O_6$ and doped with Dy^{3+} concentrations of (b) 0.6 mol%, (c) 1.0 mol% and (d) 2.0 mol%.

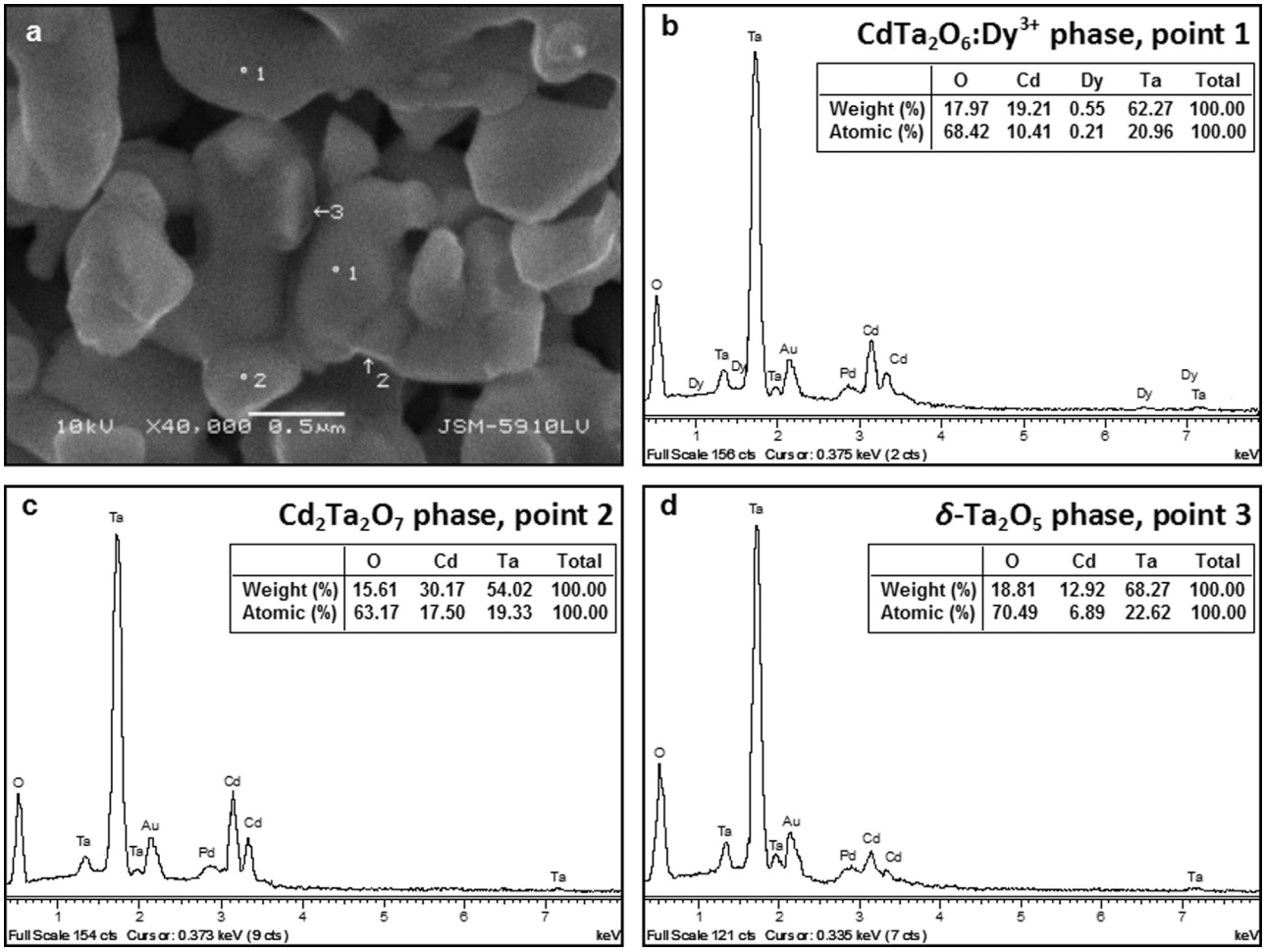

Fig. 4. SEM and EDS analyses of 2.0 mol% doped Dy^{3+} sample: (a) SEM seconder electron (SE) micrograph at magnification × 40 000 and, EDS spectra of (b) $CdTa_2O_6$ grains (point 1), (c) $Cd_2Ta_2O_7$ grains (point 2) and (d) δ-Ta_2O_5 (point 3) phase.

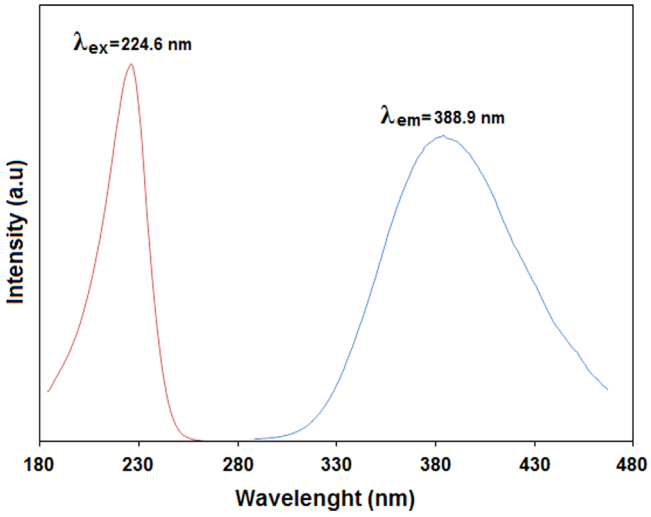

Fig. 5. Excitation peak of $CdTa_2O_6$ host located at λ_{ex}=224.6 nm and emission peak centered at λ_{em}=388.9 nm.

Fig. 6a shows the excitation spectra of $CdTa_2O_6$:xDy^{3+} (x=0.2, 0.4, 0.6, 1.0, 1.5 and 2.0 mol%) phosphors with emission monitored at 577.8 nm. The excitation spectra in the 310–440 nm range belong to the transitions between the ground level $^6H_{13/2}$ and the excited levels $^4K_{15/2}$, $^4M_{15/2}$, $^4I_{11/2}$, $^4I_{13/2}$ and $^4G_{11/2}$, respectively. The assignments of the different excitation bands were identified on the basis of Dieke's energy level diagram [44]. The excitation spectra contained five excitation bands which were observed at $^6H_{13/2}\rightarrow{}^4K_{15/2}$ (327.3 nm), $^6H_{13/2}\rightarrow{}^4M_{15/2}$ (353.0 nm), $^6H_{13/2}\rightarrow{}^4I_{11/2}$ (366.8 nm), $^6H_{13/2}\rightarrow{}^4I_{13/2}$ (388.5 nm) and $^6H_{13/2}\rightarrow{}^4G_{11/2}$ (427.4 nm) transitions. Among these excitation bands, the peak at 353.0 nm was used to investigate the photoluminescence properties of different concentrations of Dy^{3+} ions in $CdTa_2O_6$:Dy^{3+} due to sharpness and intensity of this peak.

It noticed that the CTB intensities of $CdTa_2O_6$:Dy^{3+} phosphors significantly changed depending on dopant concentration. Fig. 6b shows the CTB spectra of pure and $CdTa_2O_6$:xDy^{3+} (x=0.6, 1.0 and 2.0 mol%) samples for 388.9 nm excitation wavelength. While the CTB peak intensity for pure $CdTa_2O_6$ was found to be highest, the peak intensity of $CdTa_2O_6$:Dy^{3+} samples linearly decreases with increasing Dy^{3+} concentration up to 2 mol%. This interesting behaviour can be atributed to the crystal structure. In a study by Marciniak et al. [45] for the cubic system, the CTB intensity is strongly quenched with increasing concentration whereas for monoclinic lattice it remains practically unchanged. Similarly, it was seen that the increasing dopant concentration changed charge transfer band intensities significantly for orthorhombic columbite system.

Fig. 7a shows emission spectra of $CdTa_2O_6$:xDy^{3+} (x=0.2, 0.4, 0.6, 1.0, 1.5 and 2.0 mol%) phosphors excited at 353.0 nm. Photoluminescence spectra of $CdTa_2O_6$:Dy^{3+} phosphors exhibited two emissions that one is in blue region at 487.1 nm and the other is in yellow region at 577.8 nm. These two regions are the typical emissions of Dy^{3+} ions assigned to the transitions of $^4F_{9/2}\rightarrow{}^6H_{15/2}$

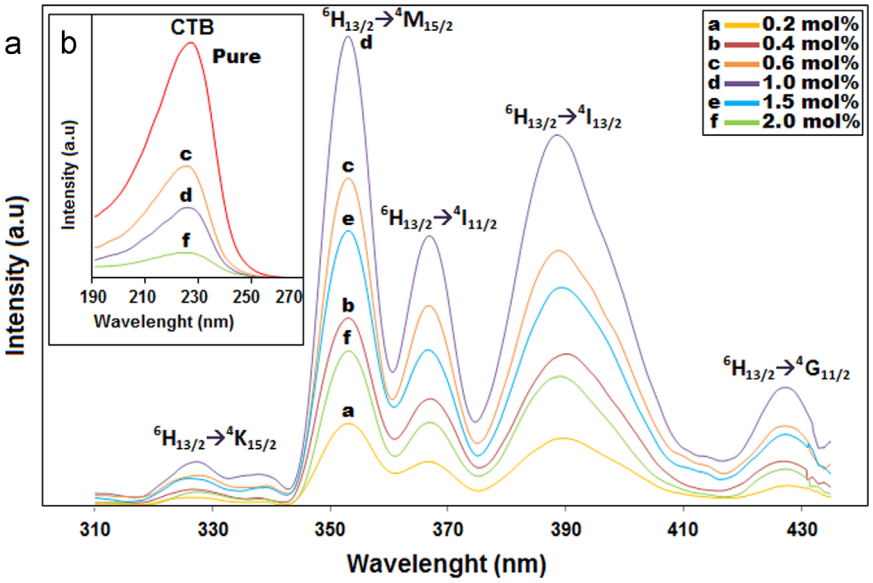

Fig. 6. Excitation spectra of (a) $CdTa_2O_6$:Dy^{3+} phosphors monitored at 577.8 nm and, the charge transfer band spectra of (b) pure $CdTa_2O_6$ and $CdTa_2O_6$:xDy^{3+} (x=c:0.6, d:1.0 and f:2.0 mol%) phosphors monitored at 388.9 nm.

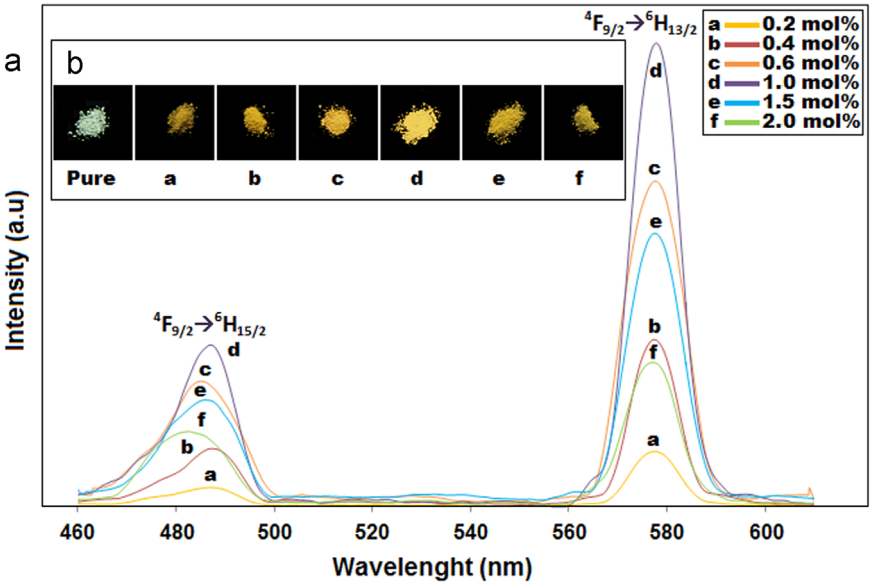

Fig. 7. Emission spectra of (a) $CdTa_2O_6$:Dy^{3+} phosphors excited at 353.0 nm and (b) the UV light photos taken by using an ultraviolet lamp as excitation source. (For interpretation of the references to color in this figure legend, the reader is referred to the web version of this article.)

and $^4F_{9/2}\rightarrow{}^6H_{13/2}$, respectively. In Fig. 7b are presented the luminescent photos for pure $CdTa_2O_6$ and $CdTa_2O_6$:Dy^{3+} samples where an ultraviolet lamp was used as an excitation source at 254 and 365 nm wavelengths, respectively. The samples were put onto quartz slide and their photos taken in a dark room.

Fig. 8 shows the dependence of emission spectra of $CdTa_2O_6$:Dy^{3+} phosphors on doping concentration. The luminescence intensity increased with the increasing Dy^{3+} concentration of up to 1.0 mol%, and then decreased because of concentration quenching effect. The quenching mechanism can be explained by two ways: (1) the impurities and structural defects, (2) the distance between RE^{3+} ions [46,47]. Accordingly, $Cd_2Ta_2O_7$, Ta_2O_5 impurities may have caused the concentration quenching effect. On the other hand, energy transfer phenomenon may be occurred by the increasing of Dy^{3+} concentration which promotes nonradiative energy transfer between Dy^{3+} ions. Therefore, excitation energy transfer depends on the critical concentration or critical distance of Dy^{3+} ions. The critical distance for energy transfer value (R_c) in $CdTa_2O_6$:Dy^{3+} can be estimated from by Blasse's equation (1) [46]:

$$R_c \approx 2\left(\frac{3V}{4\pi X_c N}\right)^{1/3} \quad (1)$$

where the structural parameters namely unit cell volume (V), the number of available sites for the dopant in the unit cell (N) and critical concentration of dopant (X_c). For the $CdTa_2O_6$:Dy^{3+} phosphor, X_c=0.01, V=445.2 (Å)^3 and N=4. The critical transfer distance (R_c) of Dy^{3+}–Dy^{3+} for $CdTa_2O_6$:Dy^{3+} phosphor was calculated as 27.71 Å.

As mentioned above, in structural analyses Dy^{3+} cations in $CdTa_2O_6$ host replaced most of the Cd^{2+} cations. According to the principle of charge balance, insertion of Dy^{3+} ions into the divalent

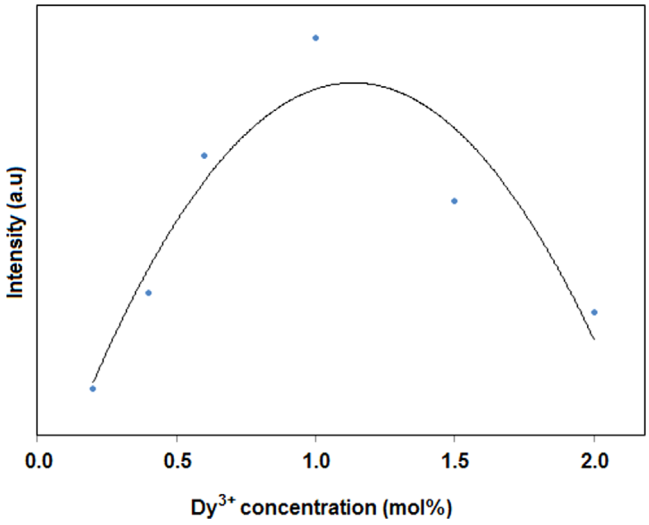

Fig. 8. Emission variation of $CdTa_2O_6$:Dy^{3+} phosphors with Dy^{3+} dopant concentration.

Cd site of $CdTa_2O_6$ structure where three Cd^{2+} ions must be replaced by two Dy^{3+} ions. During this process a cation vacancy is generated in the lattice. Therefore, when Dy^{3+} ions incorporated into $CdTa_2O_6$ host, it substitutes for a Cd^{2+} ion, which may induce structural defect $\left[Dy^{3+}\right]_{Cd}$. This is schematically represented using Kroger–Vink notation (2) as

$$CdTa_2O_6 \rightarrow V'_{Cd} + 2\left[Dy^{3+}\right]_{Cd} \quad (2)$$

where V'_{Cd} represents cadmium vacancy having two negative charges and $\left[Dy^{3+}\right]_{Cd}$ represent Dy^{3+} occupying Cd^{2+} site with extra positive charge. The vacancy may influence the luminescence intensity of the phosphor. However, charge compensation is an important factor to influence the emission efficiency of the luminescent materials [48,49].

3.3. White color properties of $CdTa_2O_6$:Dy^{3+} phosphors

It is well known that $^4F_{9/2} \rightarrow {}^6H_{15/2}$ transition gives rise to blue color. The crystal field strength around the Dy^{3+} ions hardly changes the $^4F_{9/2} \rightarrow {}^6H_{15/2}$ transition owing to the magnetic dipole transition. The site symmetry of Dy^{3+} ions is also independent in this transition when they located in the host. On the other hand, $^4F_{9/2} \rightarrow {}^6H_{13/2}$ transition leads to yellow color. The site symmetry of the Dy^{3+} ions is very sensitive to the crystal field changes owing to electric dipole transition. The emission intensity ratio of electric dipole to magnetic dipole was used to find the symmetry of the local environment of the RE^{3+} ions. When the intensity of electric dipole transition increases, asymmetry of the RE^{3+} ions will be increased. This ratio can be accepted as yellow/blue (Y/B) luminescence intensity ratio. The Y/B ratio for the $CdTa_2O_6$:Dy^{3+} phosphors indicated the presence of higher degree of interaction between dysprosium and oxygen ions [50]. It can be seen from Table 2 that there was no remarkable variation in Y/B ratio (between 1.84 and 2.05) up to 1.0 mol% Dy^{3+} ion concentration. Nevertheless, such decrease in Y/B ratio (1.78 and 1.49) for 1.5 and 2.0 mol% Dy^{3+} ion concentrations may be attributed to the secondary phase formation.

The Commission Internationale de l'Eclairage (CIE) chromaticity coordinates of $CdTa_2O_6$:Dy^{3+} phosphors with different doping concentrations under excitation at 353.0 nm were listed in Table 2. The chromaticity coordinates were determined based on their corresponding PL spectra for different concentrations of the CIE chromaticity diagram of the $CdTa_2O_6$:Dy^{3+} phosphor that was presented Fig. 9. It is seen that for all concentrations of $CdTa_2O_6$:Dy^{3+} phosphor, the estimated values were located in the white region. The chromaticity coordinates for 1.0 mol% Dy^{3+} ion doped sample was close to the standard equal energy white light (0.346, 0.419) illuminate. The present results indicated that $CdTa_2O_6$:Dy^{3+} phosphor has potential in the production of white LEDs.

In order to further examine the quality of white light, the color correlated temperature (CCT) values were calculated using McCamy empirical formula (3) and was expressed as; where $n=(x-x_e)/(y-y_e)$ is the inverse slope line, and $x_e=0.332$ and $y_e=0.186$ [51].

$$CCT = -449n^3 + 3525n^2 - 6823n + 5520.33 \quad (3)$$

The color correlated temperature (CCT) parameters of $CdTa_2O_6$:Dy^{3+} at different concentrations were presented Table 2. Generally, the preferred CCT values range from 3500 to 6500 K, but the range from 3000 to 7800 K is also acceptable. The CCT values for the $CdTa_2O_6$:Dy^{3+} phosphors were obtained in the range of 5133–6217 K. The estimated CCT data of all the samples located nearly in day light region. The CCT value for 1.0 mol% Dy^{3+} concentration was 5133 K which located in cool white daylight region.

Table 2
CIE color coordinates, CCT data and Y/B ratios of $CdTa_2O_6$ polycrystalline at different Dy^{3+} concentrations and excited at $\lambda_{ex}=353.0$ nm.

Sample	Dy^{3+} concentration (mol%)	Y/B	CIE coordinates		CCT values
			x	y	
a	0.2	1.84	0.334	0.413	5449
b	0.4	1.99	0.342	0.418	5219
c	0.6	1.94	0.340	0.416	5291
d	1.0	2.05	0.346	0.419	5133
e	1.5	1.78	0.331	0.411	5552
f	2.0	1.49	0.311	0.401	6217

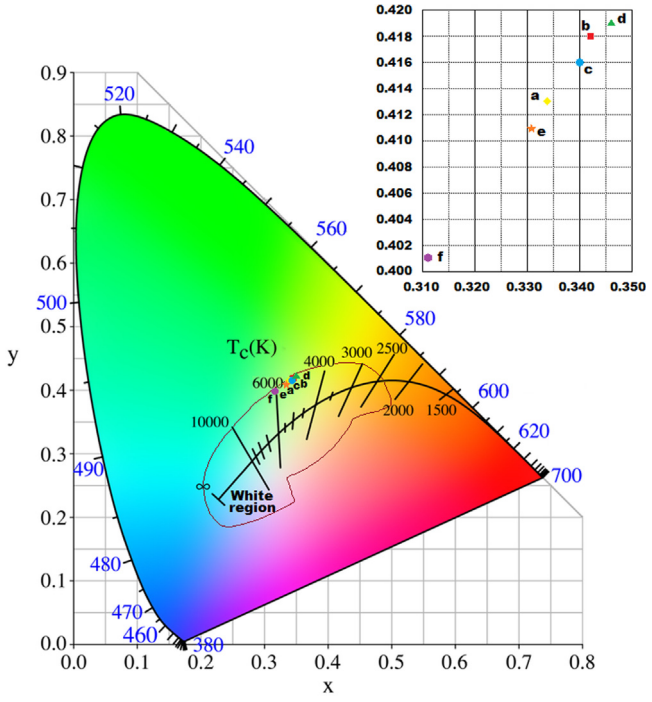

Fig. 9. CIE coordinates of the $CdTa_2O_6$:xDy^{3+} ($x=a$:0.2, b:0.4, c:0.6, d:1.0, e:1.5 and f:2.0 mol%) phosphors excited at 353.0 nm.

4. Conclusions

New light emitting Dy^{3+} doped $CdTa_2O_6$ phosphors were produced by conventional solid state method. XRD results confirmed the presence $CdTa_2O_6$ single phase having orthorhombic columbite structure that formed from 0.2 to 1.0 mol% Dy^{3+} doping concentrations. SEM analysis revealed that the grains have oval shape and grain size for all powders vary from submicron to a few microns. In EDS analysis, the elemental composition of $CdTa_2O_6$, $Cd_2Ta_2O_7$ and δ-Ta_2O_5 structures were changed depending on Ta/Cd ratio. Photoluminescence of $CdTa_2O_6$:Dy^{3+} phosphors exhibited a blue emission at $^4F_{9/2} \rightarrow {}^6H_{15/2}$ (487.1 nm) transition and a strong yellow emission $^4F_{9/2} \rightarrow {}^6H_{13/2}$ (577.8 nm) transition. While emission spectra increased between 0.2 and 1.0 mol%, after that level emission spectra decreased due to concentration quenching effect. The CIE values were near to white light point which was $x=0.346$, $y=0.419$ for 1.0 mol% Dy^{3+} doped sample. The calculated CCT data of all the phosphors located in the day light region. Based on the observed results, it was concluded that the $CdTa_2O_6$:Dy^{3+} phosphor has potential for white LED luminescence applications.

Acknowledgment

We would like to thank to Marmara University Research Fund (Project no: FEN-A-150513-0171) for the financial support for this study.

References

[1] M. Chen, T. Sun, H. Chen, Y. Zhang, L. Wu, Y. Kong, J. Xu, J. Solid State Chem. 183 (2010) 2161–2165.
[2] C.H. Park, T.H. Kim, Y. Yonesaki, N. Kumada, J. Solid State Chem. 184 (2011) 1566–1570.
[3] X. Ju, X. Li, Y. Yang, W. Li, C. Tao, W. Feng, J. Solid State Chem. 187 (2012) 109–113.
[4] H. Zhao, K. Zheng, Y. Sheng, H. Li, H. Zhang, X. Qi, Z. Shi, H. Zou, J. Solid State Chem. 210 (2014) 138–143.
[5] Y. Jia, H. Li, R. Zhao, W. Sun, Q. Su, R. Pang, C. Li, Opt. Mater. 36 (2014) 1811–1816.
[6] R. Cao, C. Cao, X. Yu, X. Sun, P. Tang, H. Ao, J. Solid State Chem. 215 (2014) 22–25.
[7] R. Cao, G. Chen, X. Yu, C. Cao, K. Chen, P. Liu, S. Jiang, J. Solid State Chem. 220 (2014) 97–101.
[8] X. Zhang, Z. Lu, F. Meng, L. Hu, X. Xu, J. Lin, C. Tang, Mater. Lett. 79 (2012) 292–295.
[9] N. Vijaya, K.U. Kumar, C.K. Jayasankar, Spectrochim. Acta Part A: Mol. Biomol. Spectrosc. 113 (2013) 145–153.
[10] T. Chengaiah, C.K. Jayasankar, K. Pavani, T. Sasikala, L.R. Moorthy, Opt. Commun. 312 (2014) 233–237.
[11] European Coordination Committee of the Radiological, Electromedical and Healthcare IT Industry, COCIR Application for New Exemption, Blvd A. Reyers 80, 1020 Brussels, 2011, pp. 1–12.
[12] V.L. Colvin, M.C. Schlamp, A.P. Alivisatos, Nature 370 (1994) 354–357.
[13] L.E. Chaar, L.A. Lamont, N.E. Zein, Renewable Sustainable Energy Rev. 15 (2011) 2165–2175.
[14] A.I. Iorgu, D. Berger, L. Alexandrescu, B.S. Vasıle, C. Matei, Chalcogenide Lett. 10 (2013) 525–531.
[15] I. Willner, R. Baron, B Willner, Biosens. Bioelectron. 22 (2007) 1841.
[16] Y.J. Choi, Y.J. Kim, J.W. Lee, Y. Lee, Y.B. Lim, H.W. Chung, J. Nanosci. Nanotechnol. 12 (2012) 2160–2168.
[17] Y. Su, Y. He, H. Lu, L. Sai, Q. Li, W. Li, L. Wang, P. Shen, Q. Huang, C. Fan, Biomaterials 30 (2009) 19–25.
[18] H. Yang, X. Liu, Z. Zhou, L. Guo, Catal. Commun. 31 (2013) 71–75.
[19] F. Haessner, G. Petzow, E. Preisler, J. Nucl. Mater. 7 (1962) 46–57.
[20] W. Jiang, W.J. Weber, J.S. Young, L.A. Boatner, J. Lian, L.M. Wang, R.C. Ewing, Nucl. Instrum. Methods Phys. Res. B 250 (2006) 188–191.
[21] M. Fischer, T. Malcherek, U. Bismayer, Phys. Rev. B 78 (2008) 014108.
[22] M.K. Ekmekçi, M. Erdem, A. Mergen, G. Özen, B. Di Bartolo, J. Alloys Compd. 591 (2014) 230–233.
[23] S.A. Ghafouri, M. Erdem, M.K. Ekmekçi, A. Mergen, G. Özen, Mater. Res. Bull. 60 (2014) 562–565.
[24] M. Thirumal, A.K. Ganguli, Prog. Cryst. Growth Charact. Mater. 44 (2002) 147–154.
[25] M. Thirumal, A.K. Ganguli, Mater. Res. Bull. 36 (2001) 2421–2427.
[26] J.H. Sturdivant, Z. Kristallogr. 75 (1930) 88–105.
[27] C.A. dos Santos, L.I. Zawislak, E.J. Kinast, V. Antonietti, J.B.M. da Cunha, Braz. J. Phys. 31 (2001) 616–631.
[28] M. İlhan, Solid State Sci. 38 (2014) 160–168.
[29] T.A. Vanderah, R.S. Roth, T. Siegrist, W. Febo, J.M. Loezos, W.W. Ng, Solid State Sci. 5 (2003) 149–164.
[30] M. Nyman, M.A. Rodriguez, L.E. Shea-Rohwer, J.E. Martin, M. Waller, F.E. Osterloh, Chem. Mater. 21 (2009) 4731–4737.
[31] M. Nyman, M.A. Rodriguez, L.E. Shea-Rohwer, J.E. Martin, P.P. Provencio, J. Am. Chem. Soc. 131 (2009) 11652–11653.
[32] S.B. Zhu, H.B. Fu, S.C. Zhang, L.W. Zhang, Y.F. Zhu, J. Photochem. Photobiol., A Chem. 193 (2008) 33–41.
[33] J. Narkilahti, M. Tyunina, J. Phys. Condens. Matter 24 (2012) 325901.
[34] A.K. Ganguli, S. Nangia, M. Thirumal, P.L. Gai, J. Chem. Sci. 118 (2006) 37–42.
[35] C.G. Almeida, H.M.C. Andrade, A.J.S. Masjarenhas, L.A. Silva, Mater. Lett. 64 (2010) 1088–1090.
[36] G.K. Layden, Mater. Res. Bull. 2 (1967) 533.
[37] W.G. Mumme, L.E. Grey, R.S. Roth, T.A. Vanderah, J. Solid State Chem. 180 (2007) 2429–2436.
[38] S.C. Navale, V. Samuel, A.B. Gaikwad, V.A. Ravi, Ceram. Int. 33 (2007) 297–299.
[39] A.I.S. Vázquez, J.J.R. Valdés, E.R. Blanco, A.Á. Méndez, S.M.D.P. Arciniega, J. Non-Cryst. Solids 380 (2013) 65–70.
[40] M. İlhan, A. Mergen, C. Yaman, Ceram. Int. 37 (2011) 1507–1514.
[41] M. İlhan, A. Mergen, C. Yaman, Ceram. Int. 39 (2013) 5741–5750.
[42] T. Dimitrova, K. Arshak, E. Atanassova, Thin Solid Films 31 (2001) 381.
[43] A.M. Srivastava, J.F. Ackerman, W.W. Beeers, J. Solid State Chem. 134 (1997) 187.
[44] G.H. Dieke, Spectra and Energy Levels of Rare Earth Ions in Crystals, Interscience Publishers, New York, 1968.
[45] L. Marciniak, M. Stefanski, R. Tomala, D. Hreniak, W. Strek, J. Alloys Compd. 624 (2015) 210–215.
[46] G. Blasse, J. Solid State Chem. 62 (1986) 207–211.
[47] J.S. Garciá, L.E. Bausá, D. Jaque, An Introduction to the Optical Spectroscopy of Inorganic Solids, John Wiley & Sons Ltd, England, 2005.
[48] F. Yang, Y. Liang, M. Liu, X. Li, N. Wang, Z. Xia, Ceram. Int. 38 (2012) 6197–6201.
[49] S. Shi, J. Gao, J. Zhou, Opt. Mater. 30 (2008) 1616–1620.
[50] [a] L. Ozawa, H. Forest, P.M. Jaffe, G. Ban, J. Electrochem. Soc. 118 (1971) 482–486;
[b] N. Vijaya, K.U. Kumar, C.K. Jayasankar, Spectrochim. Acta Part A: Mol. Biomol. Spectrosc. 113 (2013) 145–153.
[51] C.S. McCamy, Color Res. Appl. 17 (1992) 142–144.